

Sulindac selectively induces autophagic apoptosis of GABAergic neurons and alters motor behaviour in zebrafish

Received: 16 October 2022

Accepted: 22 August 2023

Published online: 02 September 2023

Check for updates

Wenwei Sun^{1,7}, Meimei Wang^{1,7}, Jun Zhao¹, Shuang Zhao¹,
Wenchao Zhu², Xiaoting Wu³, Feifei Li¹, Wei Liu¹, Zhuo Wang¹,
Meng Gao², Yiyue Zhang¹, Jin Xu¹, Meijia Zhang¹, Qiang Wang¹,
Zilong Wen^{4,5}, Juan Shen³✉, Wenqing Zhang^{1,6}✉ & Zhibin Huang¹✉

Nonsteroidal anti-inflammatory drugs compose one of the most widely used classes of medications, but the risks for early development remain controversial, especially in the nervous system. Here, we utilized zebrafish larvae to assess the potentially toxic effects of nonsteroidal anti-inflammatory drugs and found that sulindac can selectively induce apoptosis of GABAergic neurons in the brains of zebrafish larvae. Zebrafish larvae exhibit hyperactive behaviour after sulindac exposure. We also found that akt1 is selectively expressed in GABAergic neurons and that SC97 (an Akt1 activator) and exogenous akt1 mRNA can reverse the apoptosis caused by sulindac. Further studies showed that sulindac binds to retinoid X receptor alpha (RXR α) and induces autophagy in GABAergic neurons, leading to activation of the mitochondrial apoptotic pathway. Finally, we verified that sulindac can lead to hyperactivity and selectively induce GABAergic neuron apoptosis in mice. These findings suggest that excessive use of sulindac may lead to early neurodevelopmental toxicity and increase the risk of hyperactivity, which could be associated with damage to GABAergic neurons.

Nonsteroidal anti-inflammatory drugs (NSAIDs), which compose one of the largest classes of drugs worldwide, are widely applied in clinical anti-inflammatory, antipyretic and analgesic treatments. NSAIDs exert their efficacy by inhibiting the activity of cyclooxygenases (COXs), affecting the metabolism of arachidonic acid, which results in the reduction of prostaglandins and other pro-inflammatory factors in vivo¹. The most important reason for their popularity among patients

is that NSAIDs can provide quick relief from headaches and toothaches; in addition, they are affordable and easy to use. According to reports, NSAIDs are currently some of the most heavily used drugs, used by more than 30 million patients every day^{2,3}, but increasing side effects of NSAIDs have been reported after clinical application. Data from the USA FDA show that approximately 1/3 of all adverse drug reactions are caused by NSAIDs, with approximately 41,000 elderly

¹Division of Cell, Developmental and Integrative Biology, School of Medicine, South China University of Technology, Guangzhou 510006, China. ²National Engineering Research Center for Tissue Restoration and Reconstruction, Key Laboratory of Biomedical Engineering of Guangdong Province, Key Laboratory of Biomedical Materials and Engineering of the Ministry of Education, Innovation Center for Tissue Restoration Reconstruction, South China University of Technology, Guangzhou 510006, China. ³Guangdong Provincial Key Laboratory of Pharmaceutical Bioactive Substances, Guangdong Pharmaceutical University, Guangzhou 510006, China. ⁴Division of Life Science, State Key Laboratory of Molecular Neuroscience and Center of Systems Biology and Human Health, the Hong Kong University of Science and Technology, Clear Water Bay, Kowloon, Hong Kong, People's Republic of China. ⁵Greater Bay Biomedical Innocenter, Shenzhen Bay Laboratory, Shenzhen Peking University-Hong Kong University of Science and Technology Medical Center, Shenzhen 518055, China. ⁶Greater Bay Biomedical Innocenter, Shenzhen Bay Laboratory, Shenzhen 518055, China. ⁷These authors contributed equally: Wenwei Sun, Meimei Wang. ✉ e-mail: shenjuan0412@126.com; mczhangwq@scut.edu.cn; huangzhibin1986@scut.edu.cn

people hospitalized and 3300 deaths due to NSAIDs every year⁴. For example, long-term use of NSAIDs can lead to multiple-organ side effects, including gastrointestinal toxicity, cardiovascular risk, kidney injury, hepatotoxicity, and hypertension, through COX-dependent or independent pathways^{5–7}.

It should be noted that the widespread use of NSAIDs also increases the risk of acute NSAID exposure, ingestion and toxicities in pregnant women and children. For example, antenatal exposure to NSAIDs can result in a greater risk of congenital anomalies, including spina bifida⁸, premature closure of the ductus arteriosus⁹ and cardiac septal defects¹⁰. In children, recent studies have indicated that routine use or overdose of NSAIDs may cause life-threatening symptoms, such as upper gastrointestinal bleeding¹¹, acute kidney injury^{12,13} and anaphylaxis¹⁴. However, only a limited number of studies have been performed to evaluate the toxicity of NSAIDs in the nervous system¹⁵. For example, a comparative study found that overdose of NSAIDs, particularly mefenamic acid, is associated with a dose-related risk of CNS toxicity¹⁶. Therefore, exploring the adverse reaction mechanism of NSAIDs, especially during neurodevelopment, will help guide clinicians to choose drugs more accurately and reasonably. We urgently need to find a convenient way to evaluate the possible toxicity of these commonly used clinical anti-inflammatory drugs in the early developmental nervous system. Zebrafish, as emerging model organisms, have been widely used in highthroughput screening and safety evaluation of drugs due to their small size, transparent body, in vitro development, ease of drug treatment and ease of observation¹⁷. In addition, zebrafish share considerable evolutionary similarities with mammalian species. Zebrafish genes 87% homology with human genes, and their biological structures and physiological functions are highly similar to those of mammals¹⁸. Moreover, the central nervous system of zebrafish is highly homologous to that of human¹⁹. Therefore, the zebrafish model is a good choice to evaluate the neurotoxicity of NSAIDs commonly used in clinics.

In this study, acridine orange (AO) staining was carried out on zebrafish to evaluate the effects of 46 kinds of commonly used anti-inflammatory drugs or inhibitors on neurotoxicity. We found that sulindac selectively induced apoptosis of gamma-aminobutyric acid (GABA) neurons in zebrafish and mice. Zebrafish larvae exhibited hyperactive behaviour due to the loss of these inhibitory nerves. In addition, we explored the potential mechanisms of apoptosis using the autophagy inhibitor 3-methyladenine (3-MA) and SR11237, a competitive ligand against retinoid X receptor alpha (RXR α). Our results indicated that sulindac may bind to RXR α and cause autophagy-mediated apoptosis of GABAergic neurons. Collectively, the findings of this study may provide valuable insights into the underlying mechanisms of sulindac toxicity and shed light on the risks associated with NSAIDs in early neurodevelopment.

Results

Sulindac elicited neurodevelopmental toxicity

To investigate the possible toxic effects of anti-inflammatory drugs being used in clinical treatment, we conducted a small-scale anti-inflammatory drug screening for brain developmental toxicity (Fig. 1a). Zebrafish embryos were collected, and five embryos were arrayed at 2 days post-fertilization (dpf) in each well of a 24-well plate, with the compound to be tested dissolved at 10 μ M in DMSO and E3 embryo medium. The fish were then screened at 4 dpf by AO staining. To examine whether the compounds had specific effects, we retested them at varying concentrations and confirmed the zebrafish phenotypes. Finally, we screened a total of 46 NSAIDs listed in Supplementary Table 1, and only sulindac caused obvious apoptosis in the midbrains of zebrafish larvae, as indicated within the dashed lines in Fig. 1c. In contrast, DMSO (Fig. 1b, as a control group) and the other drugs, including acetaminophen (Fig. 1d), aspirin (Fig. 1e), ibuprofen (Fig. 1f), naproxen (Fig. 1g), rofecoxib (Fig. 1h) and diclofenac (Fig. 1i),

had few toxic effects. Interestingly, these apoptotic cells were specifically distributed in the midbrain, while no apparent apoptotic cells were observed in the trunk region (Supplementary Fig. 1). To further determine the cell types of apoptosis in the midbrain, neuron-labelled transgenic zebrafish *Tg(Xla.Tubb:DsRedx)* and vasculature-labelled transgenic zebrafish *Tg(flk1:mCherry)* were used to colocalize apoptotic cells (Fig. 1j, k; Supplementary Fig. 2). The results showed that the vast majority of apoptotic cells were neuronal cells, suggesting that sulindac exerts adverse effects on early neurodevelopment in zebrafish larvae.

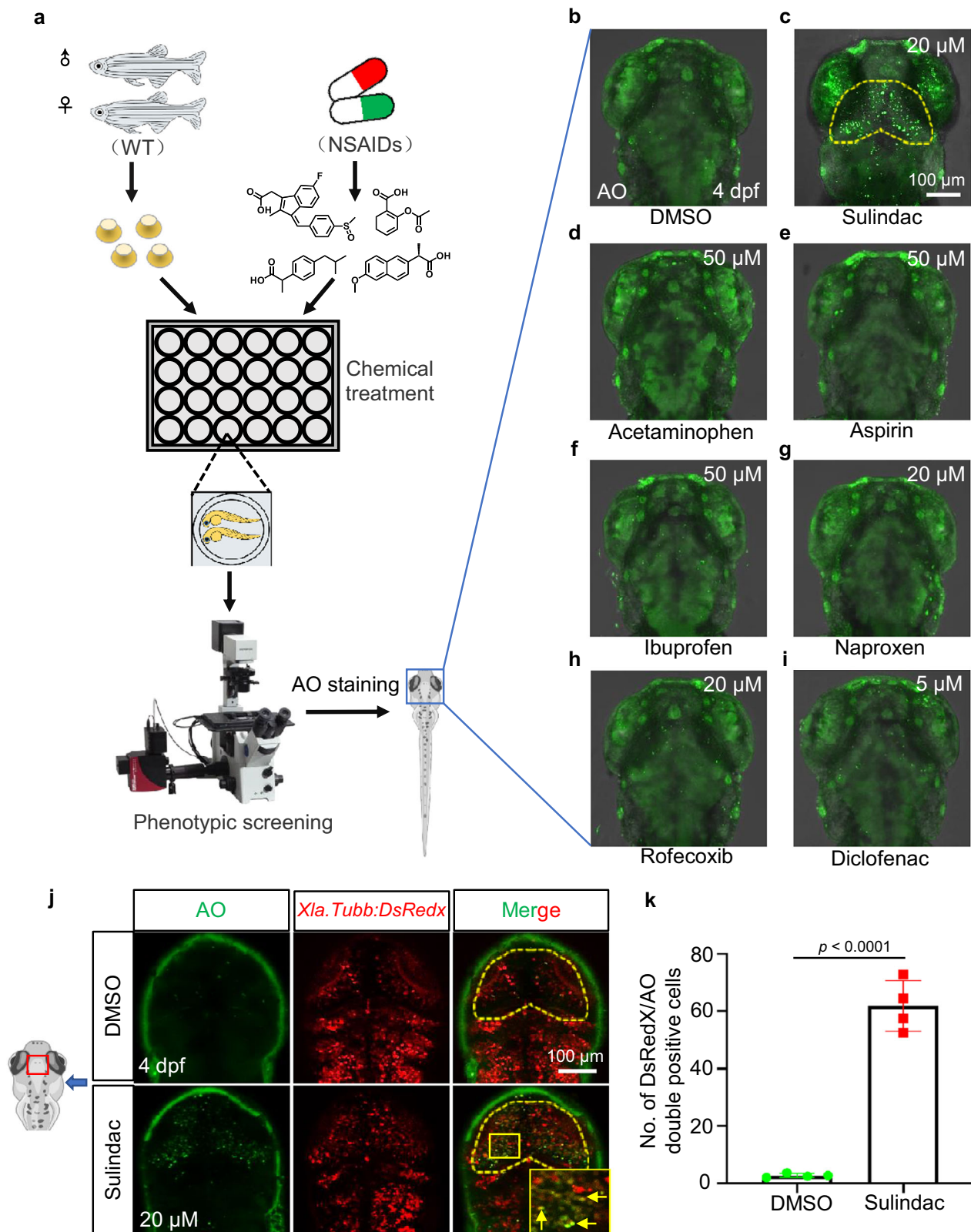
Sulindac selectively induced apoptosis of GABAergic neurons and altered motor behaviour in zebrafish larvae

To further explore which types of neurons were affected by sulindac, different types of zebrafish neuron transgenic lines were used. In particular, apoptotic cells were colocalized with mCherry⁺ GABAergic neurons in *Tg(gad1b:mCherry)* transgenic zebrafish (Fig. 2a, b) but not with glutamatergic neurons in *Tg(vglut2a:GFP)*, cranial motor neurons in *Tg(islet:GFP)* or retinal ganglion cells in *Tg(ato7:mCherry)* transgenic zebrafish (Supplementary Fig. 3a–c). Therefore, these results suggested that sulindac selectively promoted the apoptosis of GABAergic neurons. Interestingly, it has been shown that GABAergic circuitry is involved in motor behaviour²⁰. To further confirm whether the apoptosis of GABAergic neurons induced by sulindac affected the locomotor behaviour of zebrafish larvae, a photoperiod stimulation test was used to monitor the behavioural traces of larvae at 5 dpf (Fig. 2c). Records of larval motion trails showed that compared with controls, sulindac-exposed zebrafish exhibited hyperactive behaviour, especially in the highest dose group. In addition, sulindac resulted in increases in total swimming distance (11497.72 ± 1396.99 mm) and speed (3.19 ± 0.39 mm/s) in the highest dose group in comparison to the control group (6253.65 ± 674.491 mm and 1.74 ± 0.19 mm/s, respectively) during light–dark transition stimulation (Fig. 2d–g). This behaviour showed hyperactivity, which may have been attributable to the damage to GABAergic neurons caused by sulindac.

Sulindac selectively induced apoptosis of GABAergic neurons via the Akt pathway in zebrafish

As we observed that sulindac selectively induced apoptosis of GABAergic neurons in the midbrains of zebrafish larvae above, we examined the underlying mechanism of sulindac selectivity in GABAergic neurons. To do so, we identified some genes that have been reported to be associated with GABAergic neuron development, including *akt*²¹, *bdnf*²², *erbb4*²³, *fgf9*²⁴, *mtor*²⁵ and *pi3k*²⁶. Interestingly, single-cell RNA-sequencing data from the whole brains of zebrafish larvae (GEO accession GSE212888) showed that only *akt1*, a homologue of mammalian *Akt1*, but not *akt2* and *akt3*, was specifically expressed in a subpopulation of GABAergic neurons of 3-dpf zebrafish larvae (Fig. 3a, b; Supplementary Fig. 4, and Supplementary Table 2). The expression of *akt1* did not occur in many cells but was sufficient to provide a clue regarding the underlying mechanism. However, *bdnf*, *erbb4* (*erbb4a*, *erbb4b*, *ERBB4*), *fgf9*, *mtor*, and *pi3k* (*pi3ca*, *pi3cb*, *pi3cd*) were not restricted to GABAergic neurons (Fig. 3a). Furthermore, we also found that approximately 50% of *gad1b:mCherry* neurons expressed Akt1 in the zebrafish midbrain by immunofluorescence staining (Fig. 3c). AKT is a kinase with three isoforms: AKT1, AKT2 and AKT3²⁷. These isoforms are functionally distinct due to differences in target specificity^{28,29}. Emerging evidence suggests that AKT1 is highly expressed in the mammalian brain and plays a crucial role in brain development^{30,31}. Therefore, we hypothesized that Akt1 may play an important role in GABAergic neuron cell death induced by sulindac.

To further support this notion, we performed tissue-specific knockout of *akt1* in GABAergic neurons or overexpression of *akt1* to observe the apoptotic regulation of *akt1* on GABAergic neuron cell death. For tissue-specific knockout of *akt1* in GABAergic neurons, a



tissue-specific CRISPR vector (*gad1b:Cas9-T2A-mCherry, U6:gRNA akt1*) was applied^{32,33}, which contains two key promoters: one is the zebrafish U6 promoter, which can drive the expression of the guide RNA (gRNA) *akt1*, and the other is the zebrafish *gad1b* regulatory element, which tissue-specifically controls the expression of zebrafish codon-optimized Cas9 and the fluorescent reporter mCherry (Fig. 3d). To ensure the reliability of the knockout results, the knockout efficiency of the *akt1* target sequence and the CRISPR vector were verified

(Supplementary Fig. 5 and Supplementary Fig. 6). Notably, AO staining showed that tissue-specific knockout of *akt1* significantly increased the apoptosis of GABAergic neurons (Fig. 3e, f), which was also consistent with the results induced by treatment with the AKT inhibitor MK-2206 (Supplementary Fig. 7). In contrast, we found that the changes in the number of apoptotic GABAergic neurons (Fig. 3g, h) and the expression of Gad67 protein following sulindac treatment (Fig. 3i, j) were able to be reversed by overexpression of *akt1* mRNA but not by

Fig. 1 | Sulindac, identified through a small clinical anti-inflammatory drug screening, elicited neurodevelopmental toxicity. **a** Flow diagram of a small-scale anti-inflammatory drug screening for brain developmental toxicity. Wild-type (WT) embryos were collected and arrayed in 24-well plates at 2 dpf. Each well contained the compound dissolved to 10 μ M in DMSO and E3 embryo medium. Screening was conducted via acridine orange (AO) staining at 4 dpf. **b–i** Representative results of AO staining. Among the 46 anti-inflammatory drugs, only sulindac (**c**) induced apoptosis in the zebrafish midbrain (dashed line), while the other drugs, such as acetaminophen (**d**), aspirin (**e**), ibuprofen (**f**), naproxen (**g**), rofecoxib (**h**) and

diclofenac (**i**), had no significant toxic effects compared to the DMSO (**b**). The experiments were independently repeated twice with similar results, and at least six zebrafish were observed each time. **j** AO⁺ cells (green signals) were colocalized with neuronal cells (red signals) in the midbrains of *Tg(Xla.Tubb:DsRedx)* embryos indicated by yellow arrows. **k** Quantification of the yellow double-positive cells in the midbrain. The values represent the means \pm SDs ($n = 4$ larvae for per group, each dot denotes one larva). Statistics calculated by unpaired two-tailed Student's *t* test. Source data are provided as a Source Data file.

overexpression of *akt2* mRNA (Supplementary Fig. 8a–e) or *akt3* mRNA (Supplementary Fig. 8a, b, f–h). Furthermore, we found that SC97, a major activator of brain-permeable Akt1 phosphorylation³⁴, also significantly attenuated sulindac-induced GABAergic neuronal apoptosis (Supplementary Fig. 9). These data support the notion that sulindac may induce GABAergic neuron cell death by reducing p-Akt levels in the midbrains of zebrafish larvae.

Sulindac induced apoptosis via the mitochondrial pathway

To further explore the potential apoptotic mechanisms, whole-head tissue was separated for detection (Fig. 4a). We screened proteins from a series of genes that have been reported to be associated with apoptosis, including p53, Bcl-2 and Bax, poly (ADP-ribose) polymerase (PARP), caspase 3, caspase 8 and caspase 9^{35,36}. We found that the caspase cascade signalling pathway was activated, while p53 was not altered (Supplementary Fig. 10a, b). Cleaved caspase 3, cleaved caspase 9, cleaved PARP and Bax levels were increased in a dose-dependent manner (Fig. 4b–i), but the Bcl-2 level was decreased (Fig. 4b, j). Interestingly, we used a *Tg(Xla.Tubb:bcl-2)* transgenic line, in which zebrafish *bcl-2* mRNA is overexpressed specifically in neurons under the control of a *Xenopus* neuron-specific β -tubulin (*Xla.Tubb*) promoter, and Bcl-2 overexpression considerably reduced the number of apoptotic neuronal cells, which had been increased by sulindac (Fig. 4k, l). It is widely accepted that the interaction between the apoptosis-promoting factor Bax and the inhibitor of apoptosis Bcl-2 plays an important role in mitochondrial apoptosis and that Bax can directly bind to mitochondria, inducing the release of cytochrome c from mitochondria into the cytosol³⁷. Consequently, the release of cytochrome c results in the activation of the caspase cascade, including caspase 9 and caspase 3, and further amplifies the apoptotic signal³⁸. As expected, our results showed that cytochrome c accumulation in the cytoplasm was significantly increased in the sulindac group compared to the DMSO group (Fig. 4m).

The release of cytochrome c causes loss of the mitochondrial membrane potential ($\Delta\Psi$ m), which is a marker for mitochondrial dysfunction³⁹. To further confirm that sulindac-induced apoptosis was mediated by the mitochondrial pathway, changes in $\Delta\Psi$ m were analysed with flow cytometry via detection of the fluorescent dye JC-1, which produces red fluorescence when the mitochondrial membrane potential is high and green fluorescence when the mitochondrial membrane potential is low⁴⁰. Treatment with sulindac resulted in a marked collapse of $\Delta\Psi$ m in a concentration-dependent manner in zebrafish neuronal cells (Fig. 4n, o).

As sulindac is a well-known COX inhibitor, we designed specific MOs to knock down the expression of COXs (Ptgs1/Cox-1, Ptgs2a/Cox-2a and Ptgs2b/Cox-2b), but few apoptotic cells were observed after treatment with sulindac (Supplementary Fig. 11a–c), suggesting that COXs were not involved in sulindac-induced apoptosis. Prostaglandin E2 (PGE2) is the main effector prostanoid and is regulated by COXs⁴¹. However, the apoptotic effect of sulindac was not reversed by exposure to 16,16-dimethyl-PGE2 (dmPGE2; Supplementary Fig. 11d), a long-acting derivative of PGE2. Taken together, these results indicated that sulindac caused mitochondrial dysfunction and triggered Bcl2-dependent mitochondrial apoptotic pathways but not the COX-dependent pathway.

Sulindac promoted RXR α -dependent autophagy-induced apoptosis through the PI3K/AKT/mTOR pathway

Previous studies have shown that both AKT and BCL-2 play a key role in modulating the interplay between autophagy and apoptosis by negatively regulating the Beclin1-dependent autophagy program^{42,43}. The process of apoptosis is often accompanied by the occurrence of autophagy, which has a dual role in the process of apoptosis. Mild autophagy is a self-protecting process and is responsible for degrading damaged organelles and misfolded proteins, while excessive autophagy causes the destruction of a substantial number of normal organelles, leading to the activation of programmed cell death, called autophagic cell death⁴⁴. To investigate the effects of sulindac on neuronal apoptosis and autophagy in zebrafish, a red fluorescent protein (RFP)-tagged Lc3 (RFP-Lc3) plasmid was injected to mark the magnitude of autophagic flux, and AO staining was used to mark apoptotic cells⁴⁵. The results showed that both RFP-Lc3⁺ and AO⁺ cells were dramatically increased in the zebrafish midbrains after sulindac treatment (Fig. 5a, b). More interestingly, most of the RFP-Lc3⁺ cells were colocalized with AO⁺ cells. We next used electron microscopy to assess ultrastructural changes. Phenotypically, a reduced number of mitochondria and multiple small autophagosomes (Fig. 5c, green arrows), distinguished by their characteristic double membranes, were identified, as well as large autolysosomes containing electron-dense deposits (Fig. 5c, red arrows). These results further revealed that sulindac induced autophagy in neurons. Then, we explored the relationship between sulindac-induced autophagy and apoptosis by combining treatment with sulindac and 3-MA (an autophagy inhibitor) or Z-VAD-FMK (an apoptosis inhibitor). Pretreatment with 3-MA attenuated the inhibitory effect of sulindac on neuronal cell viability, but pretreatment with Z-VAD-FMK did not affect autophagy after sulindac treatment (Fig. 5a, b). These experiments demonstrated that sulindac induced Bcl-2-mediated autophagy, thereby promoting neuronal autophagic cell death.

Given the discovery of these mechanisms of sulindac, we then sought to identify the target of sulindac in activating the autophagy pathway. Here, we predicted potential targets of sulindac using the SEA Search Server database (<https://sea.bkslab.org/>), and the results showed that the three most correlated targets were prostaglandin G/H synthase 1 (PTGS1/COX-1), RXR α and prostaglandin G/H synthase 2 (PTGS2/COX-2; Supplementary Fig. 12). Since our data showed that sulindac induced neuronal apoptosis via a COX-independent pathway, we hypothesized that RXR α may serve as a target of sulindac to induce autophagic cell death. To test this possibility, we performed a docking study to evaluate the interaction of RXR α (PDB ID: Q90416) with sulindac (Zinc ID: 3786192) using the SwissDock server (<http://www.swissdock.ch/>). The results indicated that the most favourable binding modes showed four hydrogen bonds between sulindac and residues Arg405, Asn356, Arg281, and Ala436 of RXR α and a full fitness of -2523.73 kcal/mol with -7.56 kcal/mol docked free energy (Fig. 5d). It is well known that docking free energy values less than -7.0 kcal/mol indicate strong binding activity⁴⁶. Therefore, the results demonstrated that sulindac could be tightly bound to the RXR α protein.

To further confirm the interaction between sulindac and RXR α protein in the brain tissue, sulindac was biotinylated. Assuming that sulindac interacts with RXR α , RXR α should also be indirectly

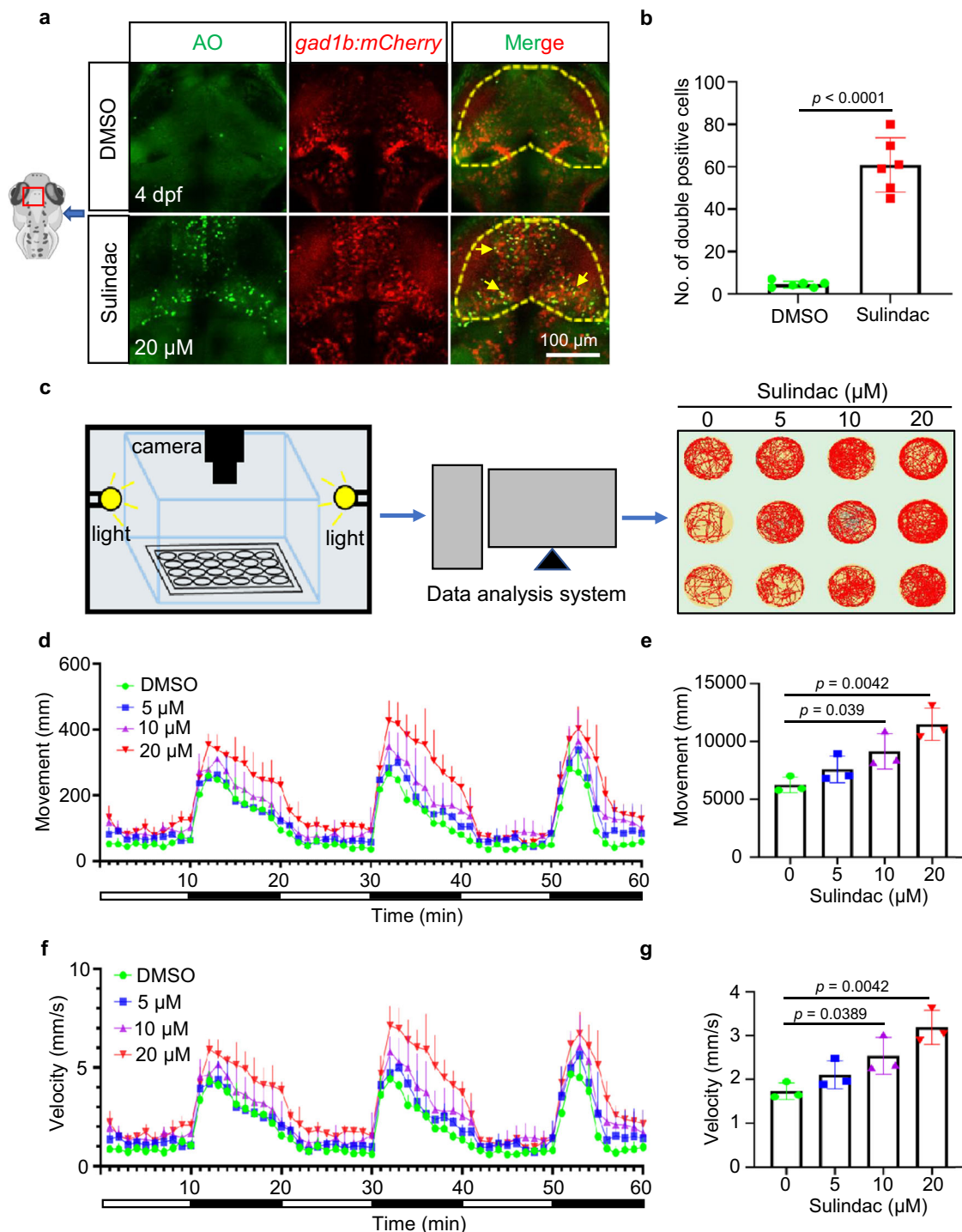


Fig. 2 | Sulindac selectively induced apoptosis of GABAergic neurons and altered motor behaviour in zebrafish larvae. **a** Most of the AO⁺ cells (green signals) were colocalized with mCherry⁺ GABAergic neurons (red signals) in the midbrains of *Tg(gad1b:mCherry)* embryos after sulindac treatment indicated by yellow arrows. **b** Quantification of the double-positive cells (yellow signals) in the midbrains of embryos. The values represent the means \pm SDs ($n = 6$ larvae per group, each dot denotes one larva). Statistics calculated by unpaired two-tailed Student's t test. Source data are provided as a Source Data file. Apoptosis of GABAergic neurons in the midbrain is indicated by yellow arrows. **c** A system of

behavioural experiments for recording larval motion trials in 60 min, and three representative photographs are shown for each group. **d**, **f** Swimming distance and velocity behavioural data were binned into 1-min intervals for analysis. The total movement (**e**) and average velocity (**g**) of zebrafish larvae exposed to sulindac at 5 dpf were examined during the light–dark photoperiod stimulation test (60 min). All data are presented as the means \pm SDs ($n = 3$ independent biological replicates, eight larvae per replicate). Statistics calculated by unpaired two-tailed Student's t test. Source data are provided as a Source Data file.

biotinylated, and therefore, the RXR α protein should be captured by the SA–biotin system⁴⁷ (Fig. 5e). As expected, the binding results showed that the amount of RXR α protein captured by sulindac–biotin was significantly increased (Fig. 5f). Together, these data imply that

RXR α may serve as an intracellular target mediating the apoptotic effect of sulindac. To further investigate the role of RXR α in sulindac-induced autophagic cell death of neurons, SRI1237 (a potent RXR α -selective ligand) was used⁴⁸. Sulindac induced extensive autophagy

Fig. 3 | Sulindac selectively induced apoptosis of GABAergic neurons via Akt signalling in zebrafish. **a** Gene dot plot showing that only *Akt1* was abundant in GABAergic neurons, but not *akt2*, *akt3a*, *akt3b*, *bdnf*, *erbb4* (*erbb4a*, *erbb4b*, *ERBB4*), *fgf9*, *mtor*, or *pi3k* (*pi3ca*, *pi3cb*, *pi3cd*). **b** Gene violin map distribution showed that *akt1* was distributed mainly in the subpopulation of GABAergic neurons. **c** Double immunostaining revealed that Akt1 proteins were selectively expressed in GABAergic neurons in the midbrains of *Tg(gad1b:mCherry)* embryos, as indicated by yellow arrows. The experiment was repeated twice with similar results, and at least five zebrafish were observed each time. **d** Flow diagram showing a tissue-specific CRISPR vector microinjected to knock out *akt1* in GABAergic neurons. **e** Specific knock out of *akt1* in GABAergic neurons via injection with the *gad1b:Cas9-T2A-mCherry,U6:gRNA akt1* vector led to apoptosis of GABAergic neurons, as indicated by yellow arrows. **f** Quantification of the yellow colour double-positive cells in the midbrains of embryos. The values represent the means \pm SDs ($n = 5$ larvae for

per group, each dot denotes one larva). Statistics calculated by unpaired two-tailed Student's *t* test. Source data are provided as a Source Data file. **g** The number of apoptotic GABAergic neurons was restored by overexpression of *akt1* mRNA after sulindac treatment, as indicated by yellow arrows. **h** Quantification of the yellow double-positive cells in the midbrains of embryos. The values represent the means \pm SDs ($n = 5$ larvae for per group, each dot denotes one larva). Statistics calculated by unpaired two-tailed Student's *t* test. Source data are provided as a Source Data file. Apoptosis of GABAergic neurons in the midbrain is indicated by yellow arrows. **i** Western blot analysis showed that overexpression of *akt1* inhibited the declines in p-Akt1 and Gad67 protein levels. **j** The data are presented as the means \pm SDs ($n = 3$ independent biological replicates). Statistics calculated by unpaired two-tailed Student's *t* test. Source data are provided as a Source Data file. β -Actin was used as an internal control.

manner, with little change in total Akt levels and Mtor levels (Fig. 5h, j). However, all these changes were reversed by SR11237. Moreover, MHY1485, an mTOR activator, significantly reversed the influence of sulindac, further supporting the notion that sulindac can arrest the PI3K/AKT/mTOR pathway, leading to the autophagic cell death of zebrafish neurons (Supplementary Fig. 13). Together, these results demonstrate that sulindac likely promotes RXR α -dependent autophagy and induces apoptosis via suppression of the PI3K/AKT/mTOR signalling pathway in zebrafish GABAergic neurons.

Long-term administration of sulindac in mice can lead to hyperactivity and apoptosis of neocortical GABAergic neurons

Based on our zebrafish findings, we decided to investigate sulindac's effects on behavioural regulation and neuronal apoptosis in mammals. Therefore, the open field test was used to evaluate the locomotor activity of mice after one month of intragastric administration of sulindac (Fig. 6a). Strikingly, we observed that the mice exhibited hyperactivity and increased excitability, as estimated by their running distance, average velocity, and frequency of centre entry (Fig. 6b–e). Interestingly, this abnormal hyperactivity became more obvious with increasing doses of sulindac (26 mg/kg, 52 mg/kg and 104 mg/kg) in mice, which was similar to the phenomenon observed in zebrafish. Therefore, these results suggest that long-term use of sulindac can lead to hyperactivity in vertebrates.

To further confirm that the autophagic cell death of GABAergic neurons was also induced by sulindac in mice, haematoxylin/eosin (H&E) staining and Nissl staining were performed and revealed that sulindac administration for 1 month also resulted in significant neuronal cell death in mice at doses of 26 mg/kg, 52 mg/kg (human equivalent dose) and 104 mg/kg (Fig. 6f–i). Moreover, consistent with the observations in zebrafish, TUNEL assays revealed that the apoptosis of GAD67-positive cells increased significantly in mice (Fig. 6j, k). All these data imply that sulindac has a potentially toxic effect on GABAergic neurons, not only in lower vertebrates but also in mammals.

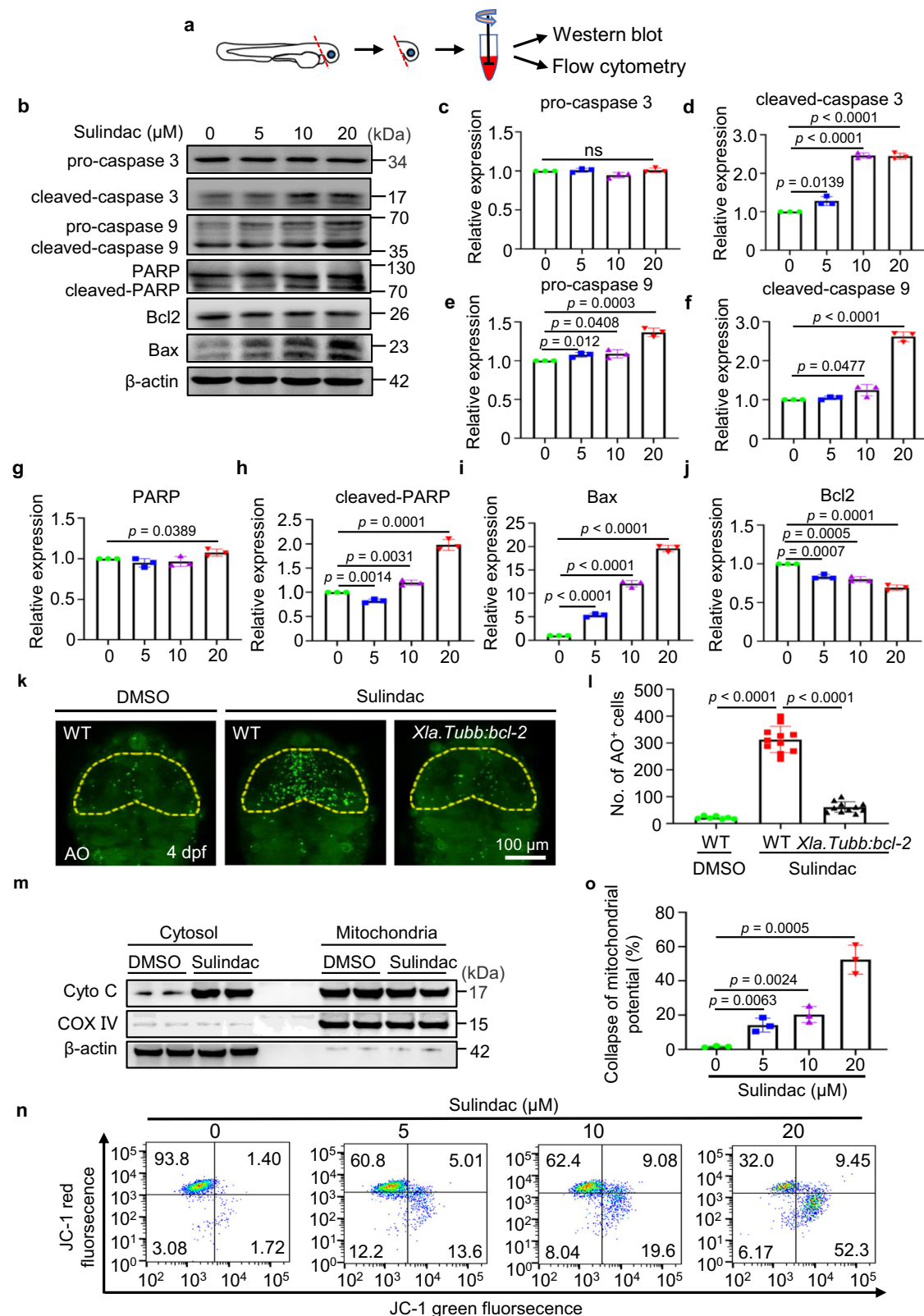
Discussion

NSAIDs play an important role in clinical medicine. They are mostly used for the treatment of patients suffering from pain and inflammatory conditions such as chronic pain, osteoarthritis, rheumatoid arthritis, postoperative surgical conditions and menstrual cramps but are even used extensively as analgesics and antipyretics⁴⁹. NSAIDs are also among the most frequently used drugs in the paediatric population^{50,51}. However, after clinical application, an increasing number of NSAIDs have been reported to cause adverse effects, including damage to the cardiac⁵², gastrointestinal⁵³, cardiovascular⁵⁴ and neurological systems of patients^{55,56}. Studies have also confirmed that overdose exposure to NSAIDs produces more serious risks to developing foetuses and children, who are even more sensitive than adults^{57,58}. However, most research on the safety of NSAIDs has focused

on foetal malformations and nephrotoxicity in children^{13,59}. In contrast, there are few studies of neurodevelopmental disorders or brain damage caused by NSAIDs, and the mechanisms underlying their effects are still unclear. Here, we report that sulindac treatment induces autophagic cell death in GABAergic neurons via the PI3K/AKT/mTOR pathway, leading to hyperactive behaviour in zebrafish larvae and mice.

GABAergic neurons are a class of inhibitory neurons in the brains of vertebrates that are mainly distributed mainly in the mature mid-brain region. They are involved in the regulation of multiple neural circuits, especially in regulating autonomic and motor behaviours⁶⁰. Recently, it was reported that disrupting the normal development of GABAergic neurons during the early developmental stage of zebrafish leads to hyperactive motor behaviours^{61,62}. Similarly, a study conducted on mice has demonstrated that dysfunction of ventral tegmental area GABA neurons can cause hyperactivity and manic-like behaviour⁶³. In our study, we found that sulindac specifically induced apoptosis of GABAergic neurons in the midbrains of zebrafish larvae through the Akt pathway, resulting in enhanced locomotor behavioural activity in zebrafish larvae and mice. AKT, a serine/threonine kinase, has been reported to selectively induce developmental defects in GABAergic neurons after knockdown of Akt in mice²¹. In addition, inhibition of Akt pathway activity has been found to result in significantly impaired development of GABAergic neurons in zebrafish larvae²⁰, which is in perfect agreement with our results. However, we were surprised to find that this restriction was reversed by overexpression of *akt1* mRNA or incubation with an AKT activator. Therefore, Akt is important for the development of GABAergic neurons, as it serves as a key regulator in the PI3K/Akt/mTOR pathway.

Sulindac, as a nonselective anti-inflammatory drug affecting COXs, is widely used for the treatment of osteoarthritis and rheumatoid arthritis. In recent years, an increasing number of studies have confirmed that there may be some COX-independent pathways involved in the pharmacological mechanism of sulindac^{64,65}. In our study, we were surprised to find that sulindac selectively induced apoptosis of GABAergic neurons. However, the downstream mechanism of sulindac remains unclear and needs to be further explored. Interestingly, RXR α , which is a unique nuclear receptor of the RXR subfamily, was predicted to be a target of sulindac by the SEA database, and accumulating evidence indicates that RXR α also has extra-nuclear functions^{66–68}. For example, RXR α migrates from the nucleus to the cytoplasm in response to differentiation⁶⁹, survival⁷⁰, apoptosis⁷¹ and inflammation⁷². Subsequently, we further confirmed strong binding between sulindac and RXR α via molecular docking and the SA-biotin system. As expected, the promoting effects of sulindac on autophagy and apoptosis were reversed by the RXR α competitive ligand SR11237, confirming that autophagy and apoptosis are directly related to the binding of sulindac and RXR α . This result is similar to the previously reported finding that sulindac can bind to RXR α and induce apoptosis in colon cancer⁷³. The PI3K/AKT/mTOR pathway plays a



major role in the processes of proliferation, apoptosis, and differentiation and is also closely related to the developing nervous system⁷⁴. Our results showed that the PI3K/AKT/mTOR pathway was suppressed by sulindac. Moreover, both additional *akt1* mRNA or activation of mTOR reversed the effects of sulindac, further supporting the hypothesis that sulindac acts by inhibiting the PI3K/AKT/mTOR pathway in the autophagic cell death process of zebrafish neurons.

Autophagy is well known as a necessary process in cell physiology and is involved in regulating both cell survival and death⁷⁵. Many studies have confirmed that autophagy has a bidirectional effect on apoptosis⁷⁶. In our study, we found that the apoptosis of GABAergic neurons induced by sulindac was also accompanied by autophagy, and 3-MA, an inhibitor of autophagy, not only significantly attenuated sulindac-induced autophagy in larval zebrafish neurons but also

Fig. 4 | Sulindac induces apoptosis via the mitochondrial pathway. **a** Schematic diagram showing that the head tissue of embryos was split for Western blotting and flow cytometry. **b** Western blot analysis of the protein levels of apoptosis-related proteins with sulindac treatment at increasing concentrations. The immunoblot intensity was determined by ImageJ analysis software. **c–j** The data are presented as the means \pm SDs ($n = 3$ independent biological replicates). NS, not significant. Statistics calculated by unpaired two-tailed Student's t test. Source data are provided as a Source Data file. β -Actin was used as an internal control. **k** After treatment with sulindac or DMSO, the number of apoptotic neurons (AO+) decreased significantly after overexpression of bcl2 in the midbrains of Tg(Xla.Tubb:bcl-2) embryos. **l** Quantification of AO+ cells in the midbrain. $n = 7$, 11 and 11 for the DMSO (WT) group, sulindac (WT) group, and sulindac (Xla.Tubb:bcl-2) group, respectively.

Each dot in **l** denotes one larva. The values represent the means \pm SDs. Statistics calculated by unpaired two-tailed Student's t test. Source data are provided as a Source Data file. **m** Western blot analysis of the protein levels of cytochrome c in the cytosolic and mitochondrial fractions of zebrafish larval neurons. The experiment was repeated three times independently with similar results. **n** Flow cytometric analysis of mitochondrial transmembrane potential ($\Delta\Psi_m$) after staining with JC-1. Zebrafish neuronal cells were treated with increasing concentrations of sulindac. **o** Quantitative data of sulindac-induced collapse of mitochondrial potential. Each column represents the mean \pm SDs ($n = 3$ independent biological replicates). Statistics calculated by unpaired two-tailed Student's t test. Source data are provided as a Source Data file.

significantly reduced neuronal apoptosis. However, the apoptosis inhibitor Z-VAD-FMK alleviated only apoptosis, not autophagy. This result suggests that sulindac treatment may activate autophagy to promote neuronal apoptosis. This is consistent with our above data that sulindac can inhibit the activity of the PI3K/AKT/mTOR pathway, leading to a reduction in the phosphorylation of mTOR (p-mTOR), followed by the occurrence of autophagy. Indeed, recent studies have revealed that the activation of the PI3K/Akt/mTOR pathway can induce autophagy via dephosphorylation of mTOR in several cell types^{77,78}. Therefore, it is possible that the occurrence of autophagy induced by sulindac is responsible for the apoptosis of GABAergic neurons.

In conclusion, our study demonstrates that sulindac triggers autophagy-mediated apoptosis of GABAergic neurons via the PI3K/AKT/mTOR pathway, resulting in hyperactive behaviour in zebrafish larvae and mice (Fig. 7). These findings suggest that prolonged use of sulindac may lead to neurotoxicity during CNS development. Thus, these results deepen our understanding of the effects of sulindac, especially in the nervous system, and should encourage more rational and effective treatments to be employed in the clinic.

Methods

Ethical statement

All experimental procedures were approved by the Institutional Animal Care and Use Committee of the South China University of Technology (approval number SCUT-2019-079).

Zebrafish maintenance

The zebrafish strains were maintained in standard laboratory conditions. The Tuebingen strain of zebrafish was used to obtain wild-type embryos, which were maintained in E2 medium at 28.5 °C and staged as previously reported⁷⁹. The following mutant and transgenic lines were used: $p53^{M214K80}$, Tg(Xla.Tubb:DsRedx)⁸¹, Tg(Xla.Tubb:bcl-2)⁸², Tg(gad1b:mCherry)⁸³, Tg(vglut2a:GFP)⁸³, Tg(ato7: mCherry)⁸⁴ and Tg(islet:GFP)⁸⁵. All experiments involving zebrafish were approved by the Institutional Animal Care and Use Committee of the South China University of Technology.

Drug exposure

Zebrafish embryos at 2 dpf were soaked in egg water containing chemicals for 2 days, and relevant experiments were performed at 4 dpf. DMSO (Sigma–Aldrich #D8418), sulindac (Selleck #S2007, 20 μ M), SR11237 (Sigma–Aldrich #S8951, 1 μ M), CD3254 (MCE #HY-107399, 1 μ M), 3-methyladenine (MCE, #HY-19312, 1 mM), Z-VAD-FMK (Selleck #S7023, 100 μ M), dmPGE2 (Apexbio #B7568, 10 μ M), MHY1485 (MCE #HY-B0795, 5 μ M), SC97 (Selleck #S7863, 1 μ M) and MK-2206 (Selleck #S1078, 30 μ M) were used in this study.

AO staining, TUNEL, H&E staining and Nissl staining

For AO staining, embryos recovered at 4 dpf were incubated in 10 μ g/mL AO stain (Sigma–Aldrich) dissolved in embryo medium in the dark for 30 min. TUNEL staining was performed with an In Situ Cell Death Detection Kit TMR red (#12156792910, Roche) as previously

described⁸⁶. H&E staining was conducted to observe the morphological and quantitative changes in neurons. Nissl staining was used to determine the loss of Nissl substance and the number of Nissl bodies. Both H&E staining and Nissl staining were performed according to standard protocols.

Immunostaining

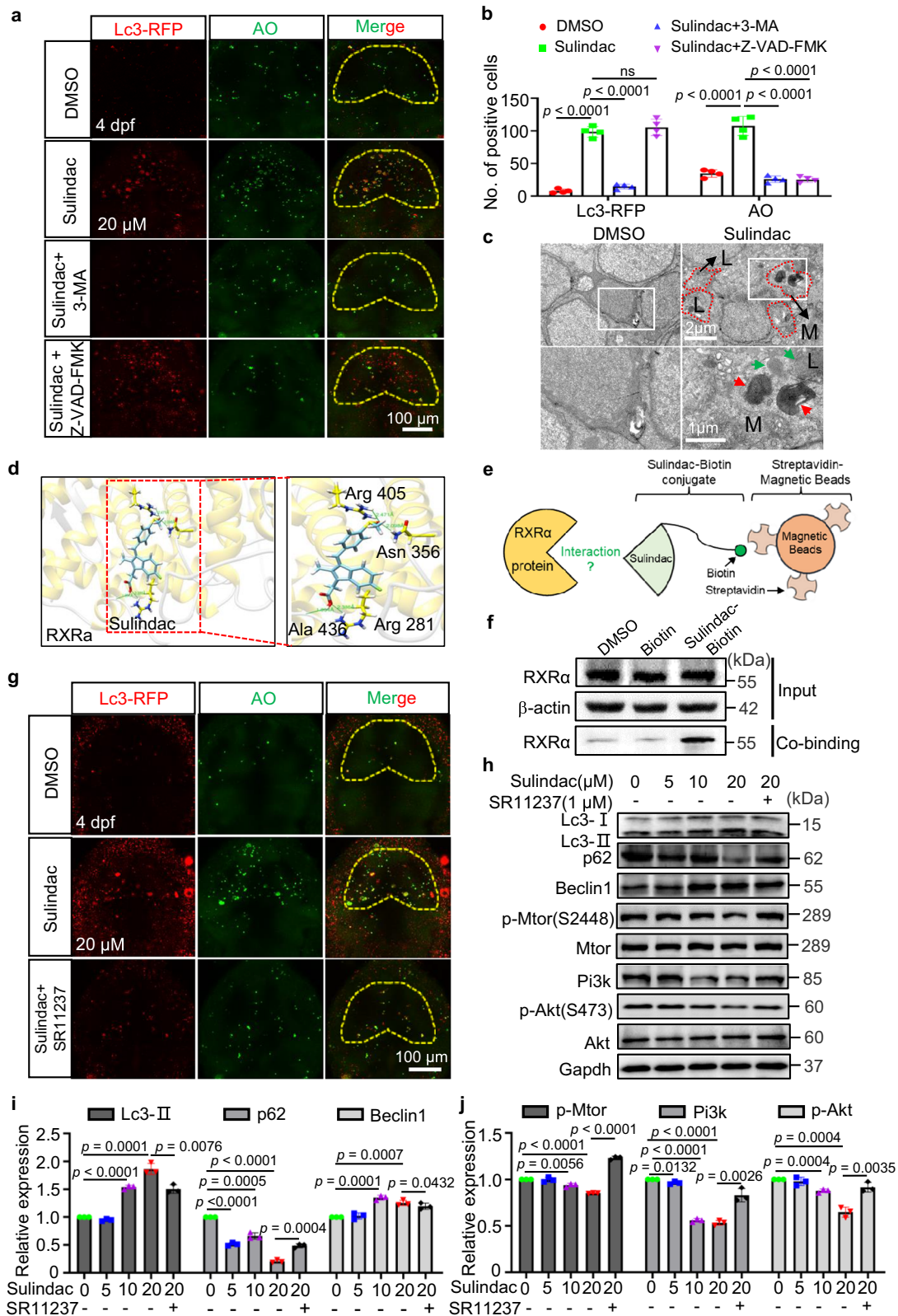
Embryos were collected and fixed overnight at 4 °C with 4% paraformaldehyde, then briefly permeabilized with methanol. Subsequently, they were rinsed and washed in PBST (PBS containing 0.1% Tween-20) to eliminate residual methanol. After blocking with blocking buffer (0.5% Triton-X PBS, 5% lamb serum, and 1% DMSO) for 2 h at room temperature, embryos were incubated with primary antibody in blocking buffer for 2 days, followed by secondary antibody for another day at 4 °C. Rabbit anti-Akt1 (Invitrogen, #PA5-29169, 1:100) and mouse anti-mCherry (Abcam, #ab125096, 1:500) were used as primary antibodies, and Alexa Fluor 488-conjugated anti-rabbit (Invitrogen, #A32731, 1:400) and Alexa Fluor 555-conjugated anti-mouse (Invitrogen, #A32727, 1:400) were used as secondary antibodies.

Single-cell gene expression quantification

The raw sequencing data were processed using Cell Ranger (v5.0) provided by 10X Genomics with the default options. The reads were aligned to the zebrafish reference transcriptome (Ensembl release 104). To ensure data quality, reads with low-quality barcodes and unique molecular identifiers (UMIs) were filtered out. For UMI counting, only reads that uniquely mapped to the transcriptome and intersected an exon by at least 50% were considered. Prior to quantification, UMI sequences were corrected for sequencing errors, and valid barcodes were identified using the EmptyDrops method⁸⁷. The resulting cell-by-gene matrices were generated through UMI counting and cell barcode assignment.

Dimensionality reduction and clustering

The resulting matrix was imported into Seurat⁸⁸ (v3.1.1) for downstream analysis. Briefly, cells that met the filter parameters of gene numbers between 200 and 3000, UMI counts <20000, and mitochondrial counts <15% were retained for subsequent analysis. Additionally, doublet GEMs were filtered out using DoubletFinder⁸⁹ (v2.0.3) with a default estimated doublet rate of 7.5%. After retaining a total of 7,758 high-quality cells, the expression values were normalized using a global-scaling method known as “Log Normalize”, which involved multiplying the total expression by a scale factor (default 10,000) and subsequently log-transforming the results. To account for batch effects and behavioural conditions on clustering, we employed Harmony to aggregate all samples⁹⁰. The Harmony algorithm takes as input a principal component analysis (PCA) embedding of cells and their corresponding batch assignments and returns a batch-corrected embedding. We performed a random permutation of a subset of the data (default: 1%), reran PCA to create a null distribution of gene scores and repeated this procedure. The identification of PCs was based on their enrichment of genes with low p values, indicating their relevance



for downstream clustering and dimensional reduction⁹¹. Euclidean distances between cells were calculated based on previously identified PCs. In brief, Seurat uses a shared-nearest neighbour (SNN) graph to embed cells, where edges are drawn between cells with similar gene expression patterns. To partition this graph into highly interconnected quasi-cliques or communities, we constructed the SNN graph based on the Euclidean distance in PCA space and refined the edge weights

between cells based on the shared overlap in their local neighbourhoods (Jaccard distance). The Louvain⁹² algorithm was employed for cell clustering and subclustering, while nonlinear dimensionality reduction (t-SNE) was used for data visualization. Subsequently, cell annotation was performed using semisupervised methods such as singleR and manual annotation. We identified and clustered four major cell types, including optic neurons, NSPCs, postmitotic neurons, and

Fig. 5 | Sulindac promoted RXRa-dependent autophagy-induced apoptosis through the PI3K/AKT/mTOR pathway in zebrafish neurons. **a** Autophagy and apoptosis were evaluated according to Lc3-RFP and AO signals when treated with 3-MA (autophagy inhibitors) or Z-VAD-FMK (apoptosis inhibitors) before sulindac treatment. **b** Quantification of Lc3-RFP+ and AO+ cells in the midbrain of embryos. The values represent the means \pm SDs ($n = 4$ larvae for per group, each dot denotes one larva). NS, not significant. Statistics calculated by unpaired two-tailed Student's t test. **c** Transmission electron micrograph analysis of autophagy measured in the midbrains of embryos treated with sulindac or DMSO. Small autophagosomes (green arrows) and autolysosomes (dashed lines) contained degraded cellular debris (red arrows), lysosomes (L), and mitochondria (M). The experiment was repeated once with similar results, and three zebrafish were observed in each group. **d** A docking study was performed to evaluate the interaction of RXRa (PDB ID: Q90416) with sulindac (Zinc ID: 3786192) via the SwissDock server (<http://www.swissdock.ch/>). The most favourable binding mode showed four hydrogen bonds

and had a full fitness of -2523.73 kcal/mol with -7.56 kcal/mol docked free energy; the close-up view is represented in the right panel. **e** Schematic diagram of the use of the streptavidin–biotin (SA–biotin) system to acquire proteins bound to sulindac. **f** Western blot analysis showed that there was an interaction between sulindac and RXRa protein in zebrafish head tissue. The experiment was repeated three times independently with similar results. **g** Autophagy and apoptosis were evaluated according to Lc3-RFP and AO signals upon treatment with SR11237 before sulindac treatment. The experiment was repeated twice with similar results, and at least five zebrafish were observed each time. **h** Western blot revealed the expression levels of autophagy-associated proteins and the PI3K/AKT/mTOR pathway proteins after treatment with increasing concentrations of sulindac as indicated. The immunoblot intensity was determined by ImageJ analysis software. **i, j** The data are presented as the means \pm SDs ($n = 3$ independent biological replicates). Statistics calculated by unpaired two-tailed Student's t test. Source data are provided as a Source Data file. GAPDH was used as an internal control.

nonneuronal cells. Furthermore, the neuronal population within the brain was reclustered into seven distinct subpopulations, resulting in a total of 22 clusters. Supplementary Table 3 provides detailed information about the cells within each cluster.

Differential expression analysis

The Wilcoxon rank-sum test⁹³ (Seurat version 3.1.1) was used for the differentially expressed gene analysis in this study. The expression values of each gene within a given cluster were compared with the rest of the cells. Significant genes were identified based on three main criteria: the genes were at least 1.28-fold overexpressed in the target cluster, the genes were expressed in more than 25% of the cells belonging to the target cluster, and the p value was less than 0.05.

Morpholino oligonucleotide (MO) injection

A previously described morpholino oligonucleotides (MO) to *ptgs1*/*cox-1* (5'-TCAGCAAAAAGTTACACTCTCTCAT-3')⁴¹, *ptgs2a*/*cox-2a* (5'-AACCAGTTTATTCATTCCAGAAGT-3')⁴¹ and *ptgs2b*/*cox-2b* (5'-AGGCTTACCTCTGTGCAAACCACG-3')⁹⁴ were purchased from Gene Tools. The MOs for *ptgs1*, *ptgs2a*, and *ptgs2b* were injected into zebrafish embryos at the one-cell stage at 300 μ M.

Synthesis of mRNA and guide RNA

The Akt coding sequence was amplified using primers (Akt1, 5'-ATG GCGACAGATGTG-3' and 5'-TCATGCTGTTCCGCT-3'; Akt2, 5'-ATGAACG AGATCAGCGTCGTC-3' and 5'-TCACTCCCGCACACTGGC-3'; Akt3a, 5'-ATGAGCGATGTCACCGTCG-3' and 5'-TCATTCTCTCCCGCTGGCC GA-3'; Akt3b, 5'-ATGAACGACCTGAACGTCGTCG-3' and 5'-TCACTCCCG CCGCTG-3'), and the PCR product was inserted into the pCS2+ vector. After linearization by NotI, the capped Akt (Akt1, Akt2, Akt3a and Akt3b) mRNA was synthesized in vitro by using an mMESSAGE mMACHINE[®] SP6 Kit (Invitrogen, #01112989) according to the manufacturer's instructions. The mRNAs were injected into each embryo at a concentration of 200 pg for Akt1, 150 pg for Akt2, and 100 pg each for Akt3a and Akt3b.

The gRNA target sites were designed using online tools (<http://chopchop.cbu.uib.no/>). The primers used for amplification of gRNA templates were as follows: T7-akt1-gRNA-F: 5'-TAATACGAC TCACTATAGGGACAATGATTACGGTCGTGGTTTTAGAGCTAGAAATA GC-3'; gRNA-R: 5'-AGCACCGACTCGGTGCCACT-3'. gRNA was transcribed using a MAXIscript T7 kit (Invitrogen, #AM1314). The Cas9 protein (NEB, Cat# M0646T), an RNA-guided endonuclease, was used to cleave the site-specific genomic DNA⁹⁵. A volume of 1 nL of a mixture of gRNA (100 pg) and Cas9 protein (500 pg) was coinjected into each single-celled embryo.

Plasmid construction

For the construction of the *cmv*:RFP-Lc3 plasmid, PCR was performed to generate RFP cDNA without the termination codon, and then

replace the EGFP coding region of pEGFP-C1, and the resulting plasmid was named RFP-C1. The fragment of Lc3 was inserted into the corresponding sites in the RFP-C1 plasmid. Finally, a 30-pg plasmid was injected into one-cell-stage embryos. For the construction of the tissue-specific CRISPR vector, we sought assistance from Professor Yang's laboratory³². The *gad1b* promoter from the transgenic line *Tg(gad1b:mCherry)* was cloned and inserted into *Cas9-T2A-mCherry,U6:gRNA(null)* to create the *gad1b:Cas9-T2A-mCherry,U6:gRNA(null)* vector by Gibson assembly reaction⁹⁶. The sequence of the *akt1* gRNA target was then inserted into the U6:gRNA cassette to construct the CRISPR vector *gad1b:Cas9-T2A-mCherry,U6:gRNA akt1*. Finally, a mixture of 100 pg of CRISPR vector and 20 pg of Tol2 mRNA was injected into one-cell-stage wild-type embryos.

Confocal imaging

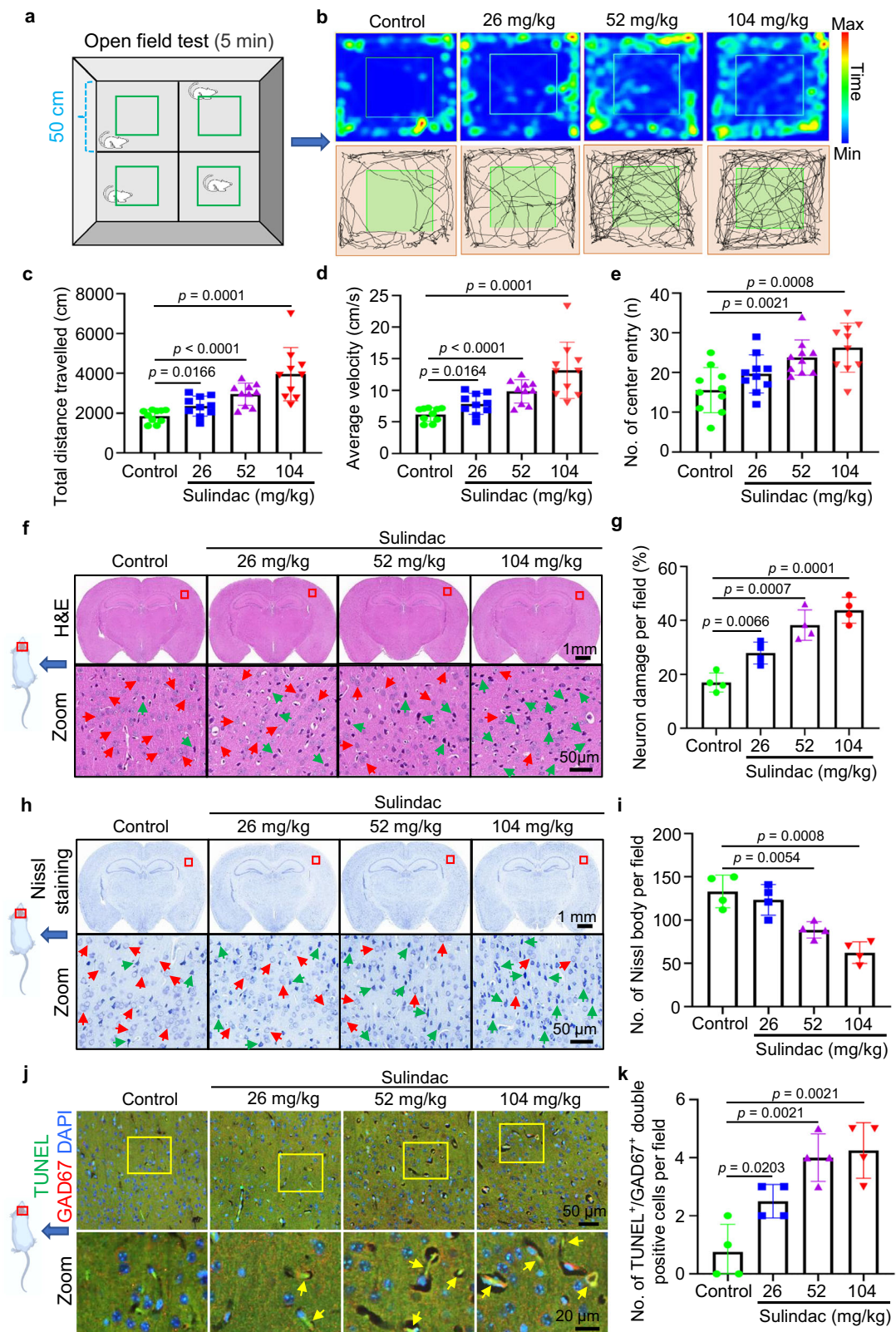
Zebrafish larvae were anaesthetised with 0.01% tricaine and mounted in 1% low-melting agarose with 0.01% tricaine. A Zeiss 800 confocal microscope was used for imaging the samples. Optical sections were obtained under a $\times 10$ or $\times 20$ air immersion objective lens at a resolution of 1024×1024 pixels, with the pinhole diameter adjusted to 1 Airy unit for each emission channel to ensure all intensity values fell within the linear range of 1 to 250. A 561-nm laser with an emission wavelength range of 570–650 nm and a 488-nm laser with an emission wavelength range of 500–550 nm were utilized. The microscope was operated on the Zeiss Zen blue 2.5 software platform (Carl Zeiss).

Detection of mitochondrial membrane potential

After drug treatment, whole-brain tissue was separated from zebrafish juveniles, and a cell suspension was prepared according to a previously described method⁹⁷. Briefly, brain tissues were dissociated with 300 μ L papain solution (28 units/mL, Worthington) containing 1% DNase and 12 mg/mL L-cysteine in DMEM/F12. The mixture was incubated at 37 °C for 15 min with gentle agitation. Dissociated cells were then washed twice with washing buffer (100 mL: 650 μ L 45% glucose, 500 μ L 1 M HEPES and 5 mL FBS into 93.85 mL 1 \times DPBS). Finally, the collected cells were incubated with JC-1 (10 mM) in the dark at 37 °C for 30 min. Finally, the changes in mitochondrial membrane potential ($\Delta\Psi_m$) were detected using flow cytometry (Beckman Coulter, USA).

Extraction of cytoplasm and mitochondria from cells

First, the cell suspension was prepared according to a previously described method⁹⁷. Briefly, brain tissues were dissociated with 300 μ L papain solution (28 units/mL, Worthington) containing 1% DNase and 12 mg/mL L-cysteine in DMEM/F12. The mixture was incubated at 37 °C for 15 min with gentle agitation. Dissociated cells were then washed twice with washing buffer (100 mL: 650 μ L 45% glucose, 500 μ L 1 M HEPES and 5 mL FBS into 93.85 mL 1 \times DPBS). Subsequently, a mitochondria isolation kit for tissue (Abcam, #ab110168) was used to obtain the cytoplasmic and mitochondrial fractions according to the



manufacturer's instructions with minor changes. Neuronal cells were homogenized in ice-cold mitochondria isolation buffer containing protease inhibitor cocktail after resuspension and then centrifuged at $1000 \times g$ for 10 min twice at $4^\circ C$ to remove debris. The supernatant was centrifuged at $12,000 \times g$ for 15 min twice to isolate the mitochondrial fraction. Finally, the resulting pellet containing mitochondria was washed twice with isolation buffer, and the remaining supernatant served as the cytosolic fraction.

Western blotting

The encephalons of 4-dpf larvae were dissected and lysed in RIPA lysis buffer supplemented with protease inhibitor cocktail (Roche, #04693116001) for Western blot analysis. The proteins were then separated by 10–13.5% SDS-PAGE and transferred to nitrocellulose (NC) membranes. The membranes were first blocked in 5% BSA and then incubated overnight at $4^\circ C$ with primary antibodies. Subsequently, the membranes were incubated with secondary antibodies for

Fig. 6 | Sulindac caused mice to display hyperactivity and induced apoptosis of neocortical GABAergic neurons. **a** Schematic diagram of the monitoring the locomotion of mice in an open field. **b–e** Hyperlocomotion of mice was manifested as increases in movement distance, average speed and the number of entries into the central area after sulindac treatment. The data are presented as the means \pm SDs ($n = 10$ mice per group). Statistics calculated by unpaired two-tailed Student's *t* test. Source data are provided as a Source Data file. **f** Haematoxylin/eosin (H & E) staining showed the structural morphology of neuronal cells in the cerebral cortex of mice after sulindac treatment. Red arrows indicate normal neuronal cells, and green arrows indicate dying neurons in the cerebral cortex in mice. **g** Quantification of dying neurons in the cerebral cortex in mice. The data are presented as the means \pm SDs ($n = 4$ mice per group). Statistics calculated by unpaired two-tailed Student's *t* test. Source data are provided as a Source Data file. **h** Nissl staining demonstrated that the Nissl bodies of

neurons were gradually lost in the cerebral cortex in mice in a dose-dependent manner after sulindac treatment. Normal neurons contained a large number of Nissl bodies (red arrow), which disappeared in dying neurons (green arrow). **i** Quantification of Nissl bodies in the cerebral cortex in mice. The data are presented as the means \pm SDs ($n = 4$ mice per group). Statistics calculated by unpaired two-tailed Student's *t* test. Source data are provided as a Source Data file. **j** Double staining of TUNEL/GAD67 in the cerebral cortex in mice. The yellow arrow indicates TUNEL/GAD67 double-positive cells. **k** Quantification of the number of TUNEL/GAD67 double-positive cells in the cerebral cortex in mice. The data are presented as the means \pm SDs ($n = 4$ mice per group). Each dot in (c–e, g, i, k) denotes one mouse. Statistics calculated by unpaired two-tailed Student's *t* test. Source data are provided as a Source Data file.

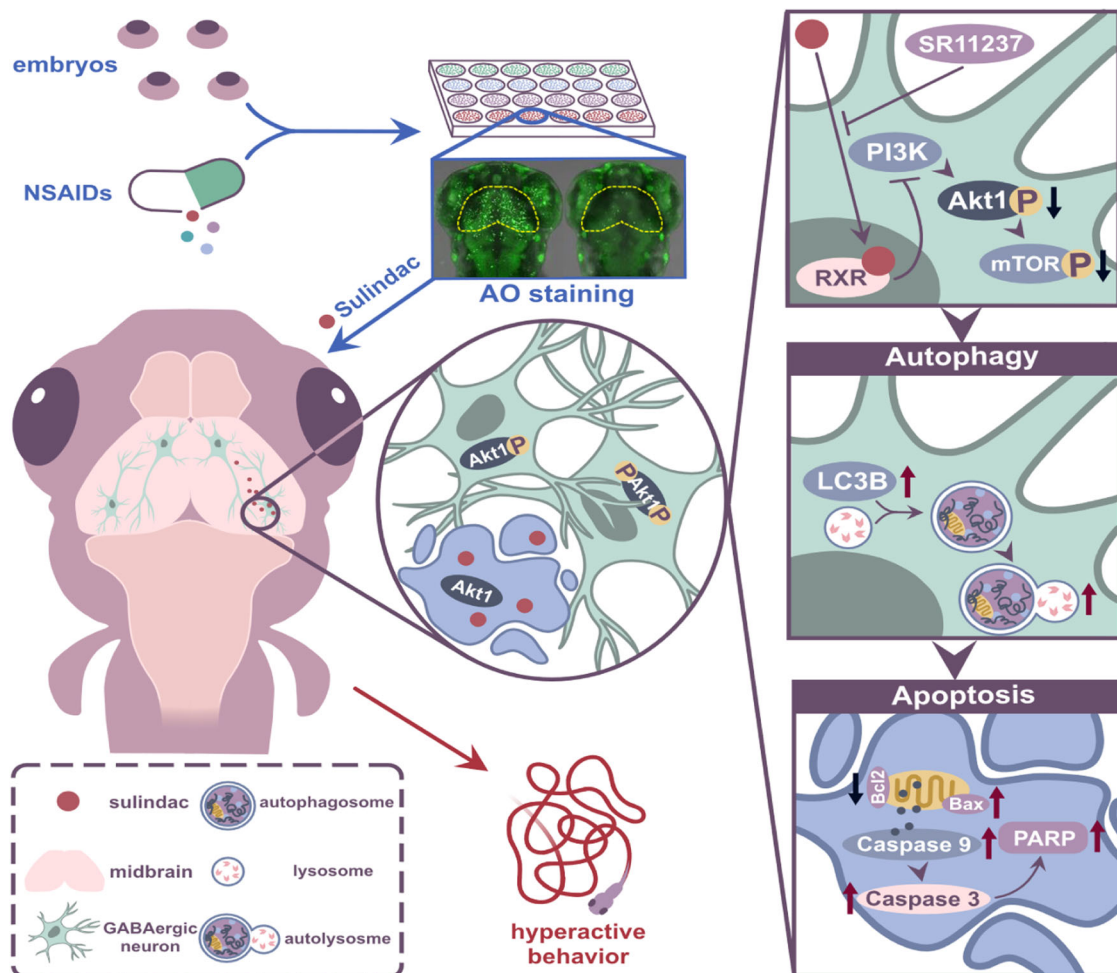


Fig. 7 | Schematic illustration of the proposed mechanisms. Sulindac treatment induces RXRa-dependent autophagic cell death in GABAergic neurons via the PI3K/AKT/mTOR pathway, leading to hyperactive behaviour in zebrafish larvae.

another 3 h. Images were visualized with a MiniChem image system (Beijing Sage Creation Science Co., China). All the information on primary antibodies is provided in Supplementary Table 4.

Detection of the interaction between sulindac and RXR α protein

A streptavidin–biotin (SA–biotin) system was utilized to confirm the interactions between sulindac and RXR α . Sulindac was biotinylated via a chemical reaction between the amino group of biotin and the carboxyl group of sulindac (Supplementary Fig. 14). Then, zebrafish embryos at 2 dpf were soaked in egg water containing biotinylated sulindac (20 μ M) for 2 days. The encephalons of 4-dpf larvae were dissected and lysed in RIPA lysis buffer supplemented with protease inhibitor cocktail (Roche, #04693116001). The protein supernatant

was obtained through low-temperature centrifugation. Subsequently, the protein mixture was transferred into a 1.5 mL microcentrifuge tube containing extensively washed streptavidin magnetic beads (Thermo Fisher, #88816) and incubated for 1.5 h at room temperature. Next, a magnetic stand was utilized to acquire target protein according to the instructions of the magnetic beads. Western blotting was used to analyse the target protein.

Determination of locomotor behaviour in larvae

All locomotor behaviour detection was performed in 24-well plates during the light phase between 9 a.m. and 4 p.m. After exposure to sulindac (5 μ M, 10 μ M, 20 μ M) or DMSO (0.1%) at 5 dpf, the free-swimming activities of zebrafish larvae in response to a 10-min light-to-

dark photoperiod stimulation were recorded with a DanioVision Observation Chamber System (Noldus IT, Netherlands). The videos were analysed using EthoVision XT software, and the total distances moved together with mean velocity were subjected to statistical analysis.

Mouse experiments

Four-week-old KM mice were obtained from Guangdong Medical Laboratory Animal Centre, Guangzhou, China. The animal licence number was SCXK (YUE) 2022-0002. All mice were housed in a facility with a light cycle running from 06:00 to 18:00, and the temperature was maintained at 20–22 °C with humidity at 50%. Food and water were available ad libitum. The mice were randomly divided into four groups ($n = 10$ per group, 5 male/5 female): saline group; sulindac groups with doses of 26 mg/kg, 52 mg/kg (human equivalent dose), and 104 mg/kg. All the mice received either sulindac or saline through gastric feeding. The treatment was repeated daily for the specified duration. After 30 days of gavage administration, behavioural monitoring experiments were performed. Subsequently, the mice were euthanized by administering with carbon dioxide for 2 min from a compressed gas tank followed by cervical dislocation, and the entire brain tissue of the mice was collected and fixed with a 4% paraformaldehyde solution for further experiments. To prepare paraffin sections, the fixed brain tissue was dehydrated with 70, 80, 95 and 100% alcohol followed by transparent with xylene, embedded in paraffin and cut into 5 μ m thickness with a microtome (Leica, Germany). For immunostaining analysis of apoptotic GAD67-positive cells, the In Situ Cell Death Detection Kit, Fluorescein (Roche, #11684795910) was used along with a polyclonal rabbit antibody to GAD67 (Abcam, #ab97739, 1:100) and anti-rabbit IgG Alexa Fluor™ 555 conjugated antibody (Invitrogen, #A31572, 1:400). The sections were mounted with VECTASHIELD containing DAPI (Vector Laboratories, #H1200). These samples were observed under an FV-1000D microscope (Olympus), and the numbers of TUNEL/GAD67 double-positive cells were counted. All animal experiments in this study were performed in strict accordance with the institutionally approved protocol according to the USPHS Guide for the Care and Use of Laboratory Animals and with the approval of the Institutional Animal Care and Use Committee of the South China University of Technology.

Locomotor activity

After one month of intragastric gavage, the locomotor activity of mice was evaluated in an open field according to a previously reported method⁹⁸. Briefly, each mouse was placed in a plastic chamber divided into a central arena and a peripheral arena with dimensions of 50 cm \times 50 cm \times 50 cm, length \times width \times height and allowed to freely explore during a 5-min session. All tests were performed in a sound-attenuated room and mouse movements were tracked with a video-tacking camera positioned above the arena using behavioural analysis software (Tracking Master V4.10 Software, Zhongshi Co., Ltd).

Statistics and reproducibility

The data are presented as the means \pm standard deviations (SDs), with sample sizes (n) provided in the text or figure legend for each experiment. Each experiment was independently repeated at least three times. All statistical analyses were performed using GraphPad Prism version 8. Two-tailed unpaired Student's t -tests were employed for comparisons between two groups, unless otherwise specified. The densities of the western blot bands were analyzed by ImageJ software.

Reporting summary

Further information on research design is available in the Nature Portfolio Reporting Summary linked to this article.

Data availability

All relevant data supporting this study are available within the paper and its supplementary information. The raw scRNA-Seq data had been deposited to the GEO database by the accession number GSE212888. Ensembl release 104 [https://ftp.ensembl.org/pub/release-104/gtf/danio_rerio/] was used to define genes for zebrafish. Source data are provided with this paper.

References

- Smith, W. L., DeWitt, D. L. & Garavito, R. M. Cyclooxygenases: Structural, cellular, and molecular biology. *Annu. Rev. Biochem.* **69**, 145–182 (2000).
- Sostres, C., Gargallo, C. J. & Lanás, A. Nonsteroidal anti-inflammatory drugs and upper and lower gastrointestinal mucosal damage. *Arthritis Res Ther.* **15**, 1–8 (2013).
- Singh, G. Gastrointestinal complications of prescription and over-the-counter nonsteroidal anti-inflammatory drugs: a view from the ARAMIS database. *Arthritis, rheumatism, and aging medical information system. Am. J. Ther.* **7**, 115–121 (2000).
- Griffin, M. R. Epidemiology of nonsteroidal anti-inflammatory drug-associated gastrointestinal injury. *Am. J. Med.* **104**, 41S–42S (1998).
- James, D. S. The multisystem adverse effects of NSAID therapy. *J. Am. Osteopath Assoc.* **99**, S1–S7 (1999).
- Werler, M. M., Mitchell, A. A., Hernandez-Diaz, S. & Honein, M. A. Use of over-the-counter medications during pregnancy. *Am. J. Obstet. Gynecol.* **193**, 771–777 (2005).
- Ilic, S. et al. Ibuprofen hepatic encephalopathy, hepatomegaly, gastric lesion and gastric pentadecapeptide BPC 157 in rats. *Eur. J. Pharm.* **667**, 322–329 (2011).
- Esposito, D. B., Parker, S. E., Mitchell, A. A., Tinker, S. C. & Werler, M. M. Periconceptional nonsteroidal anti-inflammatory drug use, folic acid intake, and the risk of spina bifida. *Birth Defects Res.* **113**, 1257–1266 (2021).
- Moise, K. J. Effect of advancing gestational age on the frequency of fetal ductal constriction in association with maternal indomethacin use. *Am. J. Obstet. Gynecol.* **168**, 1350–1353 (1993).
- Ofori, B., Oraichi, D., Blais, L., Rey, E. & Berard, A. Risk of congenital anomalies in pregnant users of non-steroidal anti-inflammatory drugs: A nested case-control study. *Birth Defects Res B Dev. Reprod. Toxicol.* **77**, 268–279 (2006).
- Grimaldi-Bensouda, L. et al. Clinical features and risk factors for upper gastrointestinal bleeding in children: a case-crossover study. *Eur. J. Clin. Pharm.* **66**, 831–837 (2010).
- Misurac, J. M. et al. Nonsteroidal anti-inflammatory drugs are an important cause of acute kidney injury in children. *J. Pediatr.* **162**, 1153–1159.e1151 (2013).
- John, C. M., Shukla, R. & Jones, C. A. Using NSAID in volume depleted children can precipitate acute renal failure. *Arch. Dis. Child* **92**, 524–526 (2007).
- Kang, L. W. et al. Severe anaphylactic reaction to ibuprofen in a child with recurrent urticaria. *Pediatrics* **120**, e742–e744 (2007).
- Wysowski, D. K. & Swartz, L. Adverse drug event surveillance and drug withdrawals in the United States, 1969–2002: the importance of reporting suspected reactions. *Arch. Intern Med* **165**, 1363–1369 (2005).
- Kamour, A. et al. Central nervous system toxicity of mefenamic acid overdose compared with other NSAIDs: an analysis of cases reported to the United Kingdom National Poisons Information Service. *Br. J. Clin. Pharm.* **83**, 855–862 (2017).
- Katoch, S. & Patial, V. Zebrafish: An emerging model system to study liver diseases and related drug discovery. *J. Appl. Toxicol.* **41**, 33–51 (2021).
- Howe, K. et al. The zebrafish reference genome sequence and its relationship to the human genome. *Nature* **496**, 498–503 (2013).

19. Kalueff, A. V., Stewart, A. M. & Gerlai, R. Zebrafish as an emerging model for studying complex brain disorders. *Trends Pharm. Sci.* **35**, 63–75 (2014).
20. Souza, B. R., Romano-Silva, M. A. & Tropepe, V. Dopamine D2 receptor activity modulates Akt signaling and alters GABAergic neuron development and motor behavior in zebrafish larvae. *J. Neurosci.* **31**, 5512–5525 (2011).
21. Oishi, K. et al. Selective induction of neocortical GABAergic neurons by the PDK1-Akt pathway through activation of Mash1. *P Natl Acad. Sci. USA* **106**, 13064–13069 (2009).
22. Turovskaya, M. V., Gaidin, S. G., Vedunova, M. V., Babaev, A. A. & Turovsky, E. A. BDNF overexpression enhances the preconditioning effect of brief episodes of hypoxia, promoting survival of GABAergic neurons. *Neurosci. Bull.* **36**, 733–760 (2020).
23. Guan, Y. F. et al. Neuregulin 1 protects against ischemic brain injury via ErbB4 receptors by increasing GABAergic transmission. *Neuroscience* **307**, 151–159 (2015).
24. Guo, M. et al. FGF9 knockout in GABAergic neurons induces apoptosis and inflammation via the Fas/caspase-3 pathway in the cerebellum of mice. *Brain Res. Bull.* **154**, 91–101 (2020).
25. Zhu, J. W. et al. Absence of TRIM32 leads to reduced GABAergic interneuron generation and autism-like behaviors in mice via suppressing mTOR signaling. *Cereb. Cortex* **30**, 3240–3258 (2020).
26. Turovsky, E. A., Turovskaya, M. V., Kononov, A. V. & Zinchenko, V. P. Short-term episodes of hypoxia induce posthypoxic hyperexcitability and selective death of GABAergic hippocampal neurons. *Exp. Neurol.* **250**, 1–7 (2013).
27. Manning, B. D. & Toker, A. AKT/PKB Signaling: Navigating the Network. *Cell* **169**, 381–405 (2017).
28. Lee, M. Y. et al. Endothelial Akt1 mediates angiogenesis by phosphorylating multiple angiogenic substrates. *Proc. Natl. Acad. Sci. USA* **111**, 12865–12870 (2014).
29. Sanidas, I. et al. Phosphoproteomics screen reveals akt isoform-specific signals linking RNA processing to lung cancer. *Mol. Cell* **53**, 577–590 (2014).
30. Balu, D. T. et al. Akt1 deficiency in schizophrenia and impairment of hippocampal plasticity and function. *Hippocampus* **22**, 230–240 (2012).
31. Yang, Z. Z. et al. Dosage-dependent effects of Akt1/protein kinase Balpha (PKBalpha) and Akt3/PKBgamma on thymus, skin, and cardiovascular and nervous system development in mice. *Mol. Cell Biol.* **25**, 10407–10418 (2005).
32. Luo, J. et al. Stepwise crosstalk between aberrant Nf1, Tp53 and Rb signalling pathways induces gliomagenesis in zebrafish. *Brain* **144**, 615–635 (2021).
33. Ablain, J., Durand, E. M., Yang, S., Zhou, Y. & Zon, L. I. A CRISPR/Cas9 vector system for tissue-specific gene disruption in zebrafish. *Dev. Cell* **32**, 756–764 (2015).
34. Liu, J. et al. Chemokine signaling synchronizes angioblast proliferation and differentiation during pharyngeal arch artery vasculogenesis. *Development* **149**, dev200754 (2022).
35. Moujalled, D., Strasser, A. & Liddell, J. R. Molecular mechanisms of cell death in neurological diseases. *Cell Death Differ.* **28**, 2029–2044 (2021).
36. Tatton, W. G., Chalmers-Redman, R., Brown, D. & Tatton, N. Apoptosis in Parkinson's disease: signals for neuronal degradation. *Ann. Neurol.* **53**, S70–62 (2003).
37. Postigo, A., Cross, J. R., Downward, J. & Way, M. Interaction of F1L with the BH3 domain of Bak is responsible for inhibiting vaccinia-induced apoptosis. *Cell Death Differ.* **13**, 1651–1662 (2006).
38. Jiang, X. & Wang, X. Cytochrome C-mediated apoptosis. *Annu Rev. Biochem.* **73**, 87–106 (2004).
39. Sasazawa, Y., Futamura, Y., Tashiro, E. & Imoto, M. Vacuolar H⁺-ATPase inhibitors overcome Bcl-xL-mediated chemoresistance through restoration of a caspase-independent apoptotic pathway. *Cancer Sci.* **100**, 1460–1467 (2009).
40. Liu, Y. et al. Hydrogen sulfide-induced oxidative stress mediated apoptosis via mitochondria pathway in embryo-larval stages of zebrafish. *Ecotoxicol. Environ. Saf.* **239**, 113666 (2022).
41. Grosser, T., Yusuff, S., Cheskis, E., Pack, M. A. & FitzGerald, G. A. Developmental expression of functional cyclooxygenases in zebrafish. *P Natl Acad. Sci. USA* **99**, 8418–8423 (2002).
42. Degtyarev, M. et al. Akt inhibition promotes autophagy and sensitizes PTEN-null tumors to lysosomotropic agents. *J. Cell Biol.* **183**, 101–116 (2008).
43. Shimizu, S. et al. Role of Bcl-2 family proteins in a non-apoptotic programmed cell death dependent on autophagy genes. *Nat. Cell Biol.* **6**, 1221–1228 (2004).
44. Heras-Sandoval, D., Perez-Rojas, J. M., Hernandez-Damian, J. & Pedraza-Chaverri, J. The role of PI3K/AKT/mTOR pathway in the modulation of autophagy and the clearance of protein aggregates in neurodegeneration. *Cell Signal* **26**, 2694–2701 (2014).
45. Chen, X. K., Kwan, J. S., Chang, R. C. & Ma, A. C. 1-phenyl 2-thiourea (PTU) activates autophagy in zebrafish embryos. *Autophagy* **17**, 1222–1231 (2021).
46. Hsin, K. Y., Ghosh, S. & Kitano, H. Combining machine learning systems and multiple docking simulation packages to improve docking prediction reliability for network pharmacology. *PLoS One* **8**, e83922 (2013).
47. Sedlak, S. M., Schendel, L. C., Gaub, H. E. & Bernardi, R. C. Streptavidin/biotin: Tethering geometry defines unbinding mechanics. *Sci. Adv.* **6**, eaay5999 (2020).
48. Gendimenico, G. J., Stim, T. B., Corbo, M., Janssen, B. & Mezick, J. A. A pleiotropic response is induced in F9 embryonal carcinoma cells and rhino mouse skin by All-trans-retinoic acid, a RAR agonist but not by SR11237, a RXR-selective agonist. *J. Invest Dermatol* **102**, 676–680 (1994).
49. Gupta, A. & Bah, M. NSAIDs in the treatment of postoperative pain. *Curr. Pain. Headache Rep.* **20**, 62 (2016).
50. Trajanovska, M., Manias, E., Cranswick, N. & Johnston, L. Use of over-the-counter medicines for young children in Australia. *J. Paediatr. Child Health* **46**, 5–9 (2010).
51. Ferreira, T. R. & Lopes, L. C. Analysis of analgesic, antipyretic, and nonsteroidal anti-inflammatory drug use in pediatric prescriptions. *J. Pediatr. (Rio J.)* **92**, 81–87 (2016).
52. Rotunno, R., Oppo, I., Saetta, G., Aveta, P. & Bruno, S. NSAIDs and heart failure: A dangerous relationship. *Monaldi Arch. Chest Dis.* **88**, 950 (2018).
53. Drmic, D. et al. Celecoxib-induced gastrointestinal, liver and brain lesions in rats, counteraction by BPC 157 or L-arginine, aggravation by L-NAME. *World J. Gastroentero* **23**, 5304–5312 (2017).
54. Olsen, A. M. et al. Cause-specific cardiovascular risk associated with nonsteroidal anti-inflammatory drugs among myocardial infarction patients—a nationwide study. *PLoS One* **8**, e54309 (2013).
55. Tyler, C. P. et al. Brain damage in preterm newborns and maternal medication: the ELGAN Study. *Am. J. Obstet. Gynecol.* **207**, 192 e191–192.e199 (2012).
56. Gervais, A. S. et al. Neurodevelopmental consequences of early plasma sodium changes in very preterm infants. *Pediatr. Res.* **92**, 1350–1356 (2022).
57. Chung, E. Y. & Tat, S. T. Nonsteroidal Anti-Inflammatory Drug Toxicity in Children A Clinical Review. *Pediatr. Emerg. Care* **32**, 250–255 (2016).
58. Titchen, T., Cranswick, N. & Beggs, S. Adverse drug reactions to nonsteroidal anti-inflammatory drugs, COX-2 inhibitors and paracetamol in a paediatric hospital. *Br. J. Clin. Pharm.* **59**, 718–723 (2005).
59. Ericson, A. & Kallen, B. A. J. Nonsteroidal anti-inflammatory drugs in early pregnancy. *Reprod. Toxicol.* **15**, 371–375 (2001).

60. Lahti, L., Achim, K. & Partanen, J. Molecular regulation of GABAergic neuron differentiation and diversity in the developing midbrain. *Acta Physiol. (Oxf.)* **207**, 616–627 (2013).
61. Barnaby, W. et al. GABAA alpha subunit control of hyperactive behavior in developing zebrafish. *Genetics* **220**, iyac011 (2022).
62. Luffe, T. M. et al. Increased locomotor activity via regulation of GABAergic signalling in foxp2 mutant zebrafish-implications for neurodevelopmental disorders. *Transl. Psychiatry* **11**, 529 (2021).
63. Yu, X. et al. Dysfunction of ventral tegmental area GABA neurons causes mania-like behavior. *Mol. Psychiatry* **26**, 5213–5228 (2021).
64. Zhang, X. P., Morham, S. G., Langenbach, R. & Young, D. A. Malignant transformation and antineoplastic actions of nonsteroidal antiinflammatory drugs (NSAIDs) on cyclooxygenase-null embryo fibroblasts. *J. Exp. Med.* **190**, 451–459 (1999).
65. Patel, M. I. et al. Celecoxib inhibits prostate cancer growth: Evidence of a cyclooxygenase-2-independent mechanism. *Clin. Cancer Res.* **11**, 1999–2007 (2005).
66. Cao, X. et al. Retinoid X receptor regulates Nur77/TR3-dependent apoptosis by modulating its nuclear export and mitochondrial targeting. *Mol. Cell. Biol.* **25**, 524–524 (2005).
67. Katagiri, Y. et al. Modulation of retinoid signalling through NGF-induced nuclear export of NGFI-B. *Nat. Cell Biol.* **2**, 435–440 (2000).
68. Zhang, X. K. et al. Regulation of the nongenomic actions of retinoid X receptor-alpha by targeting the coregulator-binding sites. *Acta Pharm. Sin.* **36**, 102–112 (2015).
69. Yang, X. H. et al. Effects of electroacupuncture and the retinoid X receptor (RXR) signalling pathway on oligodendrocyte differentiation in the demyelinated spinal cord of rats. *Acupunct. Med* **35**, 122–132 (2017).
70. Friling, S., Bergsland, M. & Kjellander, S. Activation of Retinoid X Receptor increases dopamine cell survival in models for Parkinson's disease. *BMC Neurosci.* **10**, 146 (2009).
71. Xie, C. L. et al. Steroids from the deep-sea-derived fungus penicillium granulatum MCCC 3A00475 induced apoptosis via retinoid X receptor (RXR)-alpha pathway. *Mar. Drugs* **17**, 178 (2019).
72. Paul, S., Gangwar, A., Arya, A., Bhargava, K. & Ahmad, Y. Modulation of lung cytoskeletal remodeling, RXR based metabolic cascades and inflammation to achieve redox homeostasis during extended exposures to lowered pO₂. *Apoptosis* **26**, 431–446 (2021).
73. Zhou, H. et al. NSAID sulindac and its analog bind RXRalpha and inhibit RXRalpha-dependent AKT signaling. *Cancer Cell* **17**, 560–573 (2010).
74. Tsimberidou, A. M. et al. AKT inhibition in the central nervous system induces signaling defects resulting in psychiatric symptomatology. *Cell Biosci.* **12**, 56 (2022).
75. Linder, B. & Kogel, D. Autophagy in cancer cell death. *Biol. (Basel)* **8**, 82 (2019).
76. Marino, G., Niso-Santano, M., Baehrecke, E. H. & Kroemer, G. Self-consumption: the interplay of autophagy and apoptosis. *Nat. Rev. Mol. Cell Biol.* **15**, 81–94 (2014).
77. Lin, J. F. et al. Benzyl isothiocyanate induces protective autophagy in human prostate cancer cells via inhibition of mTOR signaling. *Carcinogenesis* **34**, 406–414 (2013).
78. Singh, B. N., Kumar, D., Shankar, S. & Srivastava, R. K. Rottlerin induces autophagy which leads to apoptotic cell death through inhibition of PI3K/Akt/mTOR pathway in human pancreatic cancer stem cells. *Biochem Pharm.* **84**, 1154–1163 (2012).
79. Kimmel, C. B., Ballard, W. W., Kimmel, S. R., Ullmann, B. & Schilling, T. F. Stages of embryonic development of the zebrafish. *Dev. Dyn.* **203**, 253–310 (1995).
80. Berghmans, S. et al. tp53 mutant zebrafish develop malignant peripheral nerve sheath tumors. *Proc. Natl Acad. Sci. USA* **102**, 407–412 (2005).
81. Peri, F. & Nusslein-Volhard, C. Live imaging of neuronal degradation by microglia reveals a role for v0-ATPase a1 in phagosomal fusion in vivo. *Cell* **133**, 916–927 (2008).
82. Xu, J., Wang, T., Wu, Y., Jin, W. & Wen, Z. Microglia colonization of developing zebrafish midbrain is promoted by apoptotic neuron and lysophosphatidylcholine. *Dev. Cell* **38**, 214–222 (2016).
83. Filippi, A., Mueller, T. & Driever, W. vglut2 and gad expression reveal distinct patterns of dual GABAergic versus glutamatergic cotransmitter phenotypes of dopaminergic and noradrenergic neurons in the zebrafish brain. *J. Comp. Neurol.* **522**, 2019–2037 (2014).
84. Ng Chi Kei, J., Currie, P. D. & Jusuf, P. R. Fate bias during neural regeneration adjusts dynamically without recapitulating developmental fate progression. *Neural Dev.* **12**, 12 (2017).
85. Higashijima, S., Hotta, Y. & Okamoto, H. Visualization of cranial motor neurons in live transgenic zebrafish expressing green fluorescent protein under the control of the Islet-1 promoter/enhancer. *J. Neurosci.* **20**, 206–218 (2000).
86. Li, X., Lan, Y., Xu, J., Zhang, W. & Wen, Z. SUMO1-activating enzyme subunit 1 is essential for the survival of hematopoietic stem/progenitor cells in zebrafish. *Development* **139**, 4321–4329 (2012).
87. Lun, A. T. L. et al. EmptyDrops: distinguishing cells from empty droplets in droplet-based single-cell RNA sequencing data. *Genome Biol.* **20**, 63 (2019).
88. Butler, A., Hoffman, P., Smibert, P., Papalexi, E. & Satija, R. Integrating single-cell transcriptomic data across different conditions, technologies, and species. *Nat. Biotechnol.* **36**, 411–420 (2018).
89. McGinnis, C. S., Murrow, L. M. & Gartner, Z. J. DoubletFinder: Doublet detection in single-cell RNA sequencing data using artificial nearest neighbors. *Cell Syst.* **8**, 329–337.e324 (2019).
90. Korsunsky, I. et al. Fast, sensitive and accurate integration of single-cell data with Harmony. *Nat. Methods* **16**, 1289–1296 (2019).
91. Chung, N. C. & Storey, J. D. Statistical significance of variables driving systematic variation in high-dimensional data. *Bioinformatics* **31**, 545–554 (2015).
92. Rotta, R. & Noack, A. Multilevel local search algorithms for modularity clustering. *ACM J. Exp. Algorithmics* **16**, 2.1–2.27 (2011).
93. Camp, J. G. et al. Multilineage communication regulates human liver bud development from pluripotency. *Nature* **546**, 533–538 (2017).
94. Yeh, J. R. et al. Discovering chemical modifiers of oncogene-regulated hematopoietic differentiation. *Nat. Chem. Biol.* **5**, 236–243 (2009).
95. Gagnon, J. A. et al. Efficient mutagenesis by Cas9 protein-mediated oligonucleotide insertion and large-scale assessment of single-guide RNAs. *PLoS One* **9**, e98186 (2014).
96. Song, Y. et al. GABAergic neurons and their modulatory effects on GnRH3 in Zebrafish. *Endocrinology* **158**, 874–886 (2017).
97. Zhang, H. et al. The landscape of regulatory genes in brain-wide neuronal phenotypes of a vertebrate brain. *Elife* **10**, e68224 (2021).
98. Haba, R. et al. Lipopolysaccharide affects exploratory behaviors toward novel objects by impairing cognition and/or motivation in mice: Possible role of activation of the central amygdala. *Behav. Brain Res.* **228**, 423–431 (2012).

Acknowledgements

This work was supported by the National Key R&D Program of China (2018YFA0801000) to W.Q.Z. and Z.B.H., National Natural Science Foundation of China (32170830) to Z.B.H., National Science Foundation of Guangdong Province, China (2021A1515010422) to Z.B.H., and Fundamental Research Funds for the Central Universities (2022ZYGXZR031) to Z.B.H.

Author contributions

W.W.S. and M.M.W. designed and did most of the experiments with help from J.Z., W.C.Z., and X.T.W. helped perform the mouse experiments

and the zebrafish behavioural experiments; W.W.S. and Z.B.H. designed experiments, interpreted data, and wrote the manuscript; S.Z. dissected the brain tissues and performed the scRNA-seq. W.L., S.Z., and F.F.L. analyzed the scRNA-seq data. W.L., S.Z., and F.F.L. do the single cell analysis; M.J.Z., Q.W., Z.L.W., Z.W., W.Q.Z., M.G., Y.Y.Z., J. X., J. S., and Z.B.H. discussed the results and provided critical advice.

Competing interests

The authors declare no competing interests.

Additional information

Supplementary information The online version contains supplementary material available at <https://doi.org/10.1038/s41467-023-41114-y>.

Correspondence and requests for materials should be addressed to Juan Shen, Wenqing Zhang or Zhibin Huang.

Peer review information *Nature Communications* thanks Carsten Drepper, and the other, anonymous, reviewer(s) for their contribution to the peer review of this work.

Reprints and permissions information is available at <http://www.nature.com/reprints>

Publisher's note Springer Nature remains neutral with regard to jurisdictional claims in published maps and institutional affiliations.

Open Access This article is licensed under a Creative Commons Attribution 4.0 International License, which permits use, sharing, adaptation, distribution and reproduction in any medium or format, as long as you give appropriate credit to the original author(s) and the source, provide a link to the Creative Commons license, and indicate if changes were made. The images or other third party material in this article are included in the article's Creative Commons license, unless indicated otherwise in a credit line to the material. If material is not included in the article's Creative Commons license and your intended use is not permitted by statutory regulation or exceeds the permitted use, you will need to obtain permission directly from the copyright holder. To view a copy of this license, visit <http://creativecommons.org/licenses/by/4.0/>.

© The Author(s) 2023